DOI 10.1007/s11062-018-9721-7
Neurophysiology, Vol. 50, No. 2, April, 2018

Respiratory Rhythm in a Simplified Respiratory Network Model

Y. Zhang[1], Sh. Liu[1], and D. Xiong[2]

Received December 26, 2016

The regulatory mechanism of the respiratory system is always a hot topic in the neurobiology field. Many researchers proposed multitudinous respiratory network models and explored their internal connections. For further understanding the effect of the respiratory system in breathing, we have built a simplified respiratory network model and studied the relations between each neuron in this network. We, firstly, removed the pre-I neuron from the network and found that there are abundant bifurcation phenomena with respect for the interspike intervals (ISIs). In addition, a large number of unusual firing patterns were observed in the network under conditions of AC stimulation. After adjusting the potassium conductance in the pre-I neuron by a different tonic drive from the d_1 input, we show the transition from bursting patterns to analogous single spiking and, subsequently, convert-bursting patterns. Moreover, when sodium ion channels were removed or synaptic connections and tonic drives in the network were excluded, the network activity showed relevant variations. This may help to explain some functions of ion channels or certain neurons of the network. Finally, the biparametric screening plane with the excitatory synaptic conductance and persistent sodium conductance has been drawn. Graduations in this plane reflected different firing patterns, such as tonic spiking, bursting, and aperiodic bursting. Our results provide important insights for understanding the regulatory mechanisms of the respiratory network and the surrounding structures.

Keywords: respiratory network model, firing pattern, interspike intervals, ion channels, pre-I neuron.

INTRODUCTION

The respiratory rhythm generator in vertebrates is located in particular regions of the lower brainstem [1–4], and this rhythm is generated by special neural circuits functionally and spatially organized within this part of the brain and qualified as the respiratory central pattern generator (CPG) [5–9]. Although still insufficiently interpreted, the genesis of primary respiratory oscillations is likely to be defined, to a great extent, by the intrinsic network properties of the neurons within the above limited area. The control of breathing behavior involves a larger network distributed in different parts of the CNS and including the medulla, pons, cerebellum, and neocortex [10–12].

In previous studies, researchers have tried to completely remove the pons from the above integral system, which resulted in a gasping-like pattern of respiration [13–17]. They confirmed that the *in vitro* breathing rhythm essentially differs from that in the eupnea state, and that reduced medullary preparations without the pons cannot generate the eupneic pattern [18, 19].

In recent years, some researches paid more attention to the properties of the respiratory networks than to those of a single respiratory neuron. Jeffrey et al. [20] reviewed a hybrid pacemaker network model that, theoretically, was able to provide rhythm generation in different functional states. Yaroslav et al. [21] developed a computational model of the closed-loop respiratory system (brainstem respiratory network controlling the pulmonary subsystem) where the lung biomechanics and gas (O_2 and CO_2) exchange and transport were taken into account. Rubin et al. [22] described a reduced model that maintained the essential features and architecture of a large-scale model to elucidate the mechanisms and dynamics of synchronization between the RTN/pFRG and BötC/pre-BötC oscillations. Understanding the intricate mechanisms of the CPG and effects of recombination of its components, which provides self-adaption of rhythmic activity to different

[1] School of Mathematics, South China University of Technology, Guangzhou, China.
[2] School of Materials Science and Engineering, South China University of Technology, Guangzhou, China.
Correspondence should be addressed to Sh. Liu (e-mail: mashqliu@scut.edu.cn).

conditions, is a dominant and ambitious theme in neuroscience.

In this paper, we analyze a computational model of a simplified respiratory network and compare its behavior under different conditions with both existing experimental data and results of our experiments performed for appraising some modeling predictions. The model is considered a basis for future interactive modeling/experimental studies of the role of the pons in the generation of respiratory rhythm.

METHODS

The spatially organized model of the respiratory network represents a simplified version of the inchoate computational model. The model presented here contains four neurons ($i \in \{1, 2, 3, 4\}$) and three sources of excitatory drive (d_k; $k \in \{1, 2, 3\}$) (see Fig. 1). Among four neurons, there are one excitatory neuron and three inhibitory neurons, namely the pre-I neuron (i = 1), early-I neuron (i = 2), post-I neuron (i = 3), and aug-E neuron (i = 4).

The membrane potential V_1 to V_4 for these neurons N_1 to N_4 corresponds to the following differential equations:

$$\dot{V}_1 = \left(-I_{Na_1} - I_{NaP} - I_K - I_{L_1} - I_{SynE_1} - I_{SynI_1} + I_{app}\right)/C$$

$$\dot{V}_2 = \left(-I_{Na_2} - I_{AD_2} - I_{L_2} - I_{SynE_2} - I_{SynI_2}\right)/C$$

$$\dot{V}_3 = \left(-I_{AD_3} - I_{L_3} - I_{SynE_3} - I_{SynI_3}\right)/C$$

$$\dot{V}_4 = \left(-I_{AD_4} - I_{L_4} - I_{SynE_4} - I_{SynI_4}\right)/C$$

In the aforementioned equations, C is the membrane capacitance, I_{NaP} is the persistent sodium current, I_K is the potassium delayed-rectifier current, I_{Li} ($i \in \{1, 2, 3, 4\}$) is the leakage current; and I_{SynEi} and I_{SynIi} ($i \in \{1, 2, 3, 4\}$) are the excitatory and inhibitory synaptic currents, respectively. We added a sodium current I_{Na} for N_1 and N_2 and a gate variable n based on the literature data [23] to the original basis. These currents are described as follows:

$$I_{Na_i} = \bar{g}_{Na} m_{\infty Na}^3 (1-n)\left(V_i - E_{Na}\right)$$

$$I_{NaP} = \bar{g}_{NaP} m_{\infty NaP} h_{NaP}\left(V_1 - E_{Na}\right)$$

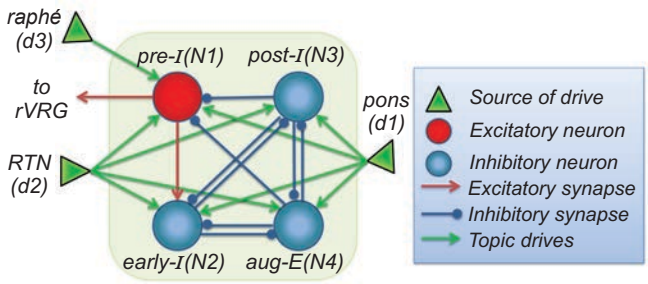

Fig. 1. Schematic diagram of the four-neuron core model of the brainstem respiratory network. Circles represent neurons (excitatory: red; inhibitory: blue); green triangles represent three sources of tonic excitatory drives (in pons, RTN, and raphé) to different neural populations. Excitatory and inhibitory synaptic connections are indicated by red or green arrows and small blue circles, respectively.

$$I_k = \bar{g}_K n^4 \left(V_1 - E_K\right)$$

$$I_{AD_i} = \bar{g}_{AD} m_{AD_i}\left(V_i - E_K\right)$$

$$I_{L_i} = \bar{g}_L \left(V_i - E_L\right)$$

$$I_{SynE_i} = \bar{g}_{SynE}\left(V_i - E_{SynE}\right)\sum_{k=1}^{3} c_{ki} d_k, i \neq 2$$

$$I_{SynE_2} = \bar{g}_{SynE}\left(V_2 - E_{SynE}\right)\left[a_{12} f_1\left(V_1\right) + \sum_{k=1}^{3} c_{ki} d_k\right]$$

$$I_{SynI_i} = \bar{g}_{SynI}\left(V_i - E_{SynI}\right)\sum_{j=2, j\neq i}^{4} b_{ji} f_j\left(V_j\right)$$

$$I_{app} = A\cos(ft)$$

where $\bar{g}_{NaP}$, $\bar{g}_k$, $\bar{g}_{AD}$, $\bar{g}_L$, $\bar{g}_{SynE}$, and $\bar{g}_{SynI}$ are the maximal conductances of the corresponding currents; E_{Na}, E_K, E_L, E_{SynE}, and E_{SynI} are the corresponding reversal potentials; a_{12} defines the weight of the excitatory synaptic input from the pre-I to the early-I neuron (see Fig. 1); b_{ji} defines the weight of the inhibitory input from neuron j to neuron i ($i \in \{1, 2, 3, 4\}$, $j \in \{2, 3, 4\}$), and c_{ki} defines the weight of the excitatory synaptic input to neuron i from drive k (d_k, $k \in \{1, 2, 3\}$). The external stimulation I_{app} defaults to zero.

The nonlinear function $f_i(V_i)$ defines the output activity of each neuron (indirectly representing the rate of spiking activity):

$$f_i\left(V_i\right) = 1/\{1 + \exp[-(V_i - V_{1/2})/k_{V_i}]\} \quad i \in \{1,2,3,4\},$$

where $V_{1/2}$ is the half-activity voltage, and k_{Vi} defines the slope for the output function for each neuron.

The voltage-dependent variables are described as follows:

$$\dot{h}_{NaP} = \left(h_{\infty NaP}\left(V_1\right) - h_{NaP}\right) / \tau_{hNaP}\left(V_1\right)$$
$$\dot{m}_{AD_i} = \left(k_{AD_i} f_i\left(V_i\right) - m_{AD_i}\right) / \tau_{AD_i}$$
$$\dot{n}_i = \alpha_n\left(V_i\right)\left(1 - n_i\right) - \beta_n\left(V_i\right) n_i \,.$$

Voltage-dependent activation and inactivation variables and time constants are described as follows:

$$m_{\infty NaP} = 1 / \{1 + exp[-(V_1 + 40) / 6]\}$$
$$m_{\infty Na} = 1 / \{1 + exp[-(V_i + 34) / 5]\}$$
$$h_{\infty NaP} = 1 / \{1 + exp[(V_1 + 48) / 6]\}$$
$$\tau_{hNaP} = \tau_{hNaPmax} / cosh[(V_1 + 48) / 12]$$
$$a_n(V_1) = (1/20) exp[(V_1 + 29) / 8]$$
$$\beta_n(V_1) = (1/20) exp[-(V_1 + 29) / 8] \,.$$

The specific parameter values of the model can be retrieved in the literature [24].

Simulations were conducted in Python and XPP using a fourth-order Runge-Kutta method with a time step of 0.1 msec. The results were processed in Origin to understand them more precisely. Numerical results have already been repeatedly verified.

RESULTS

Firing Patterns of the Pre-I Neuron, which Is Taken Away from the Network. Specifically, the excitatory pre-I neuron in our model has intrinsic oscillatory properties defined by I_{NaP} [27]. Obviously, the firing patterns of a single neuron manifest more regular phenomena, as compared to those of the network. To understand the effect of different parameters on the single pre-I neuron, we removed it from the network and made sure it has nothing to do with the network.

Values of the sodium equilibrium potential E_{Na} and potassium equilibrium potential E_K were chosen to be depicted. The results are shown in Fig. 2. These two parameters can introduce the pre-I neuron in such a regimen that it demonstrates abundant phenomena with slight differences. The diagrams A and B are the membrane potentials at the respective values of E_{Na} and E_K corresponding to the ISIs sequences (panels C and D, respectively). Whereas the E_{Na} in this neuron decreases approximately from 65 to 60 mV, the ISI sequences showed a clear period-doubling phenomenon. As the E_{Na} was less than 60 mV, the bifurcation pattern turned into a chaotic mode. Once the E_{Na} became less than 56 mV, the bifurcation pattern jumped out of the chaotic state and entered the inverse period-doubling bifurcation mode, which ultimately stayed in period-4 bursting. The firing pattern related to the E_K is similar to that at E_{Na}. While the E_K changed from –95 to –87 mV, the bifurcation pattern was similar to those determined by the E_{Na}. This also appeared as a clear period-doubling phenomenon and a series of chaotic-mode spiking. Once the E_K crossed the 87 mV level, the ISI sequences turned into a clear period-adding bifurcation. These luxuriant firing characters may be associated with intrinsic biophysical properties of the respiratory neurons.

Influence of Alternating Current (AC) Stimulation on Variation of the Firing Pattern in the Network. In previous physiological experiments, AC stimulation was found to be an essential method in modulation of neuronal network activity in humans and mammals [28-31]. Alternating current stimulation to each neuron in the network can induce a large number of disparate firing shapes. The membrane potentials have been drawn by setting the amplitude and frequency of AC stimulation.

As can be seen in Fig.3, all the above six diagrams illustrate irregular and periodic bursting. For convenience, the value of time per graph already includes at least two or three periods. Firstly, we compared panels A and B, in which AC stimulation had the same amplitude but different frequency. The oscillating period in A is tenfold greater than that in B, and the intensity of bursting is weakened along with a frequency increase. The next comparison of A and D is for conditions of the same frequency but different amplitudes. It can be observed that an increase in the amplitude also crippled the oscillation frequency. In general, diagrams A-F display a great diversity of the phenomena under different AC values. These peculiar firing patterns may give us some idea of the relations between the distinct stimulus and activity of the respiratory network.

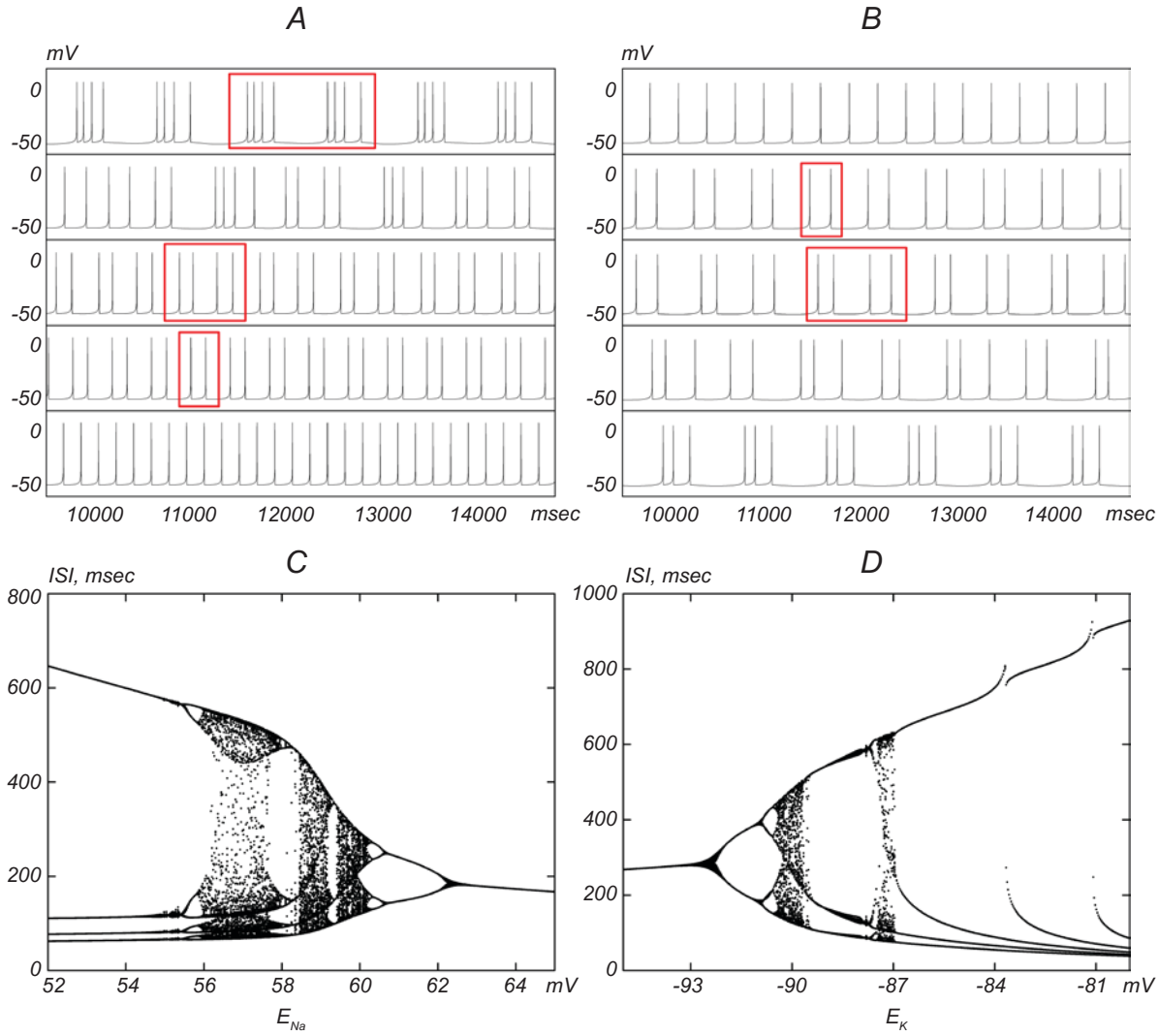

F i g. 2. Dynamic behaviors of pre-I neuron. A) Membrane potentials, from top to bottom, when E_{Na} = 55.8 mV (period-8 bursting), E_{Na} = 58.7 mV (chaotic bursting), E_{Na} = 60.4 mV (period-4 bursting), E_{Na} = 61 mV (period-2 bursting), and E_{Na} = 64 mV (single spiking), respectively. B) Membrane potentials, from top to bottom, when E_k = –93 mV (spiking), E_k = –91.5 mV (period-2 bursting), E_k = –90.6 mV (period-4 bursting), E_k = –90 mV (chaotic bursting), E_k = –89 mV (period-3 bursting), respectively. C) Graph of the ISIs *vs*. E_{Na}. The range is from 52 to 65 mV. D) Graph of the ISIs *vs.* E_K. The range is from –95 to –80 mV.

Influence of a Tonic Drive d_1 on Variations of the Firing Pattern in the Network. Many researchers have examined the effects of tonic drive in recent years [7, 21, 22, 24]. For example, the removal of the pontine input to the medullary circuits leads to the generation of an apneustic breathing pattern characterized by a significant increase in the duration of inspiration and a significant reduction of the oscillation frequency.

For further understanding of the role of the tonic drive d1 in the network activity, we firstly set the potassium conductance g_k to 8 nS (Fig.4). Then, we began to examine the tonic drive d_1 value, which comes from the pons. The d_1 value was firstly set to 0.3 (the diagram corresponds to A), and in this case the network exhibited the bursting pattern. The connection and transition between the bursts are smooth. Yet, from the diagram (B) corresponding to the d_1 value 0.6, it can be observed that the connection between bursts became oscillating. As the d_1 value continued to increase (to a 1.5 value), the bursting patterns were transformed into periodic firing, which is similar in some aspect to single spiking. A further increment of the d_1 value led to transformation of the firing patterns into bursting again, and the period became shorter. At the same time, in the entire network it can be found that when the N_1 and N_2 neurons continued the normal firing,

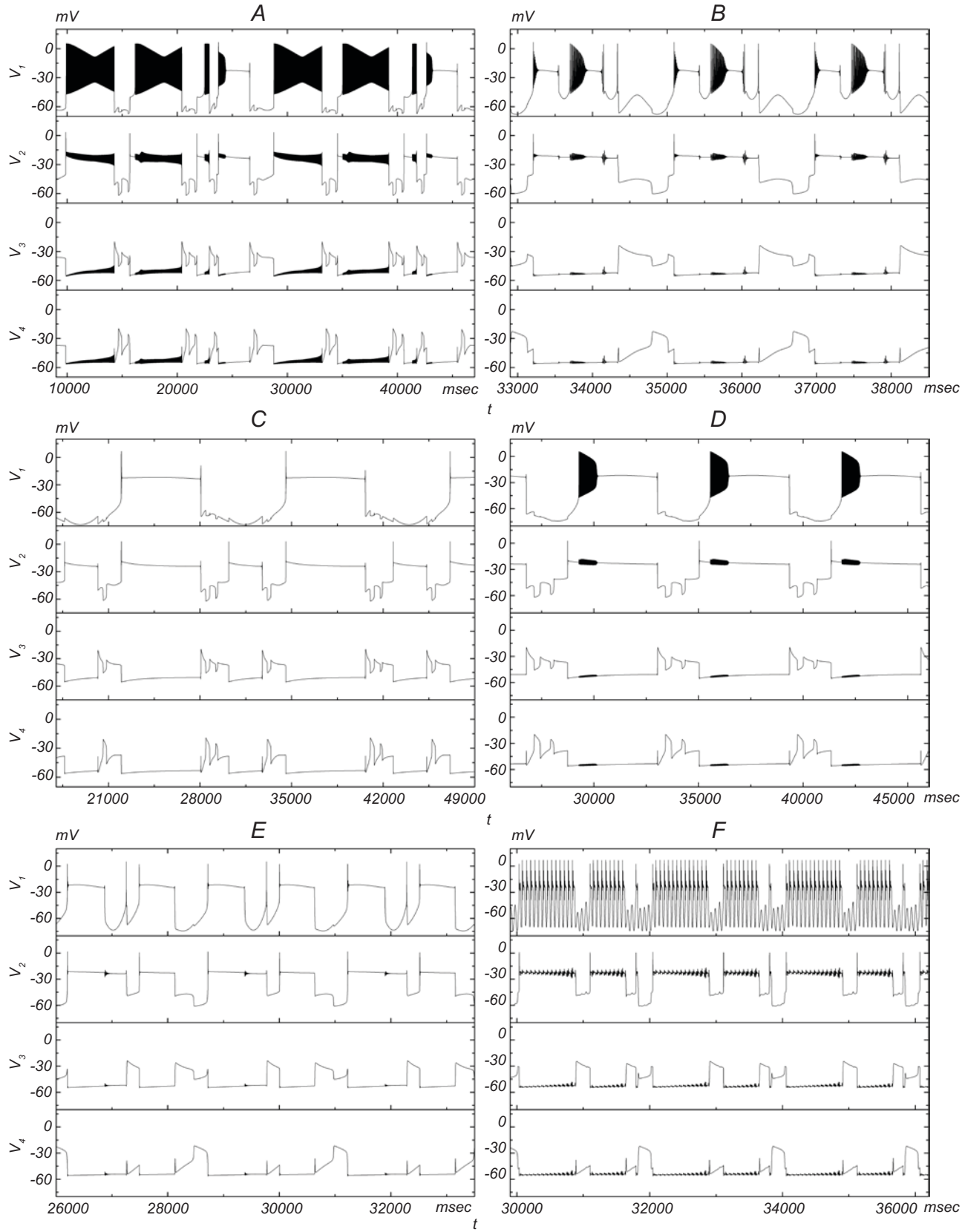

F i g. 3. Neural action potentials under different strengths of AC stimulation. For the diagrams A-F, the value of AC stimulus strength (A, f) is (100, 0.001), (100, 0.01), (200, 0.0005), (200, 0.001), (200, 0.005), and (200, 0.1) respectively. Designations A and f represent the amplitude and frequency, respectively.

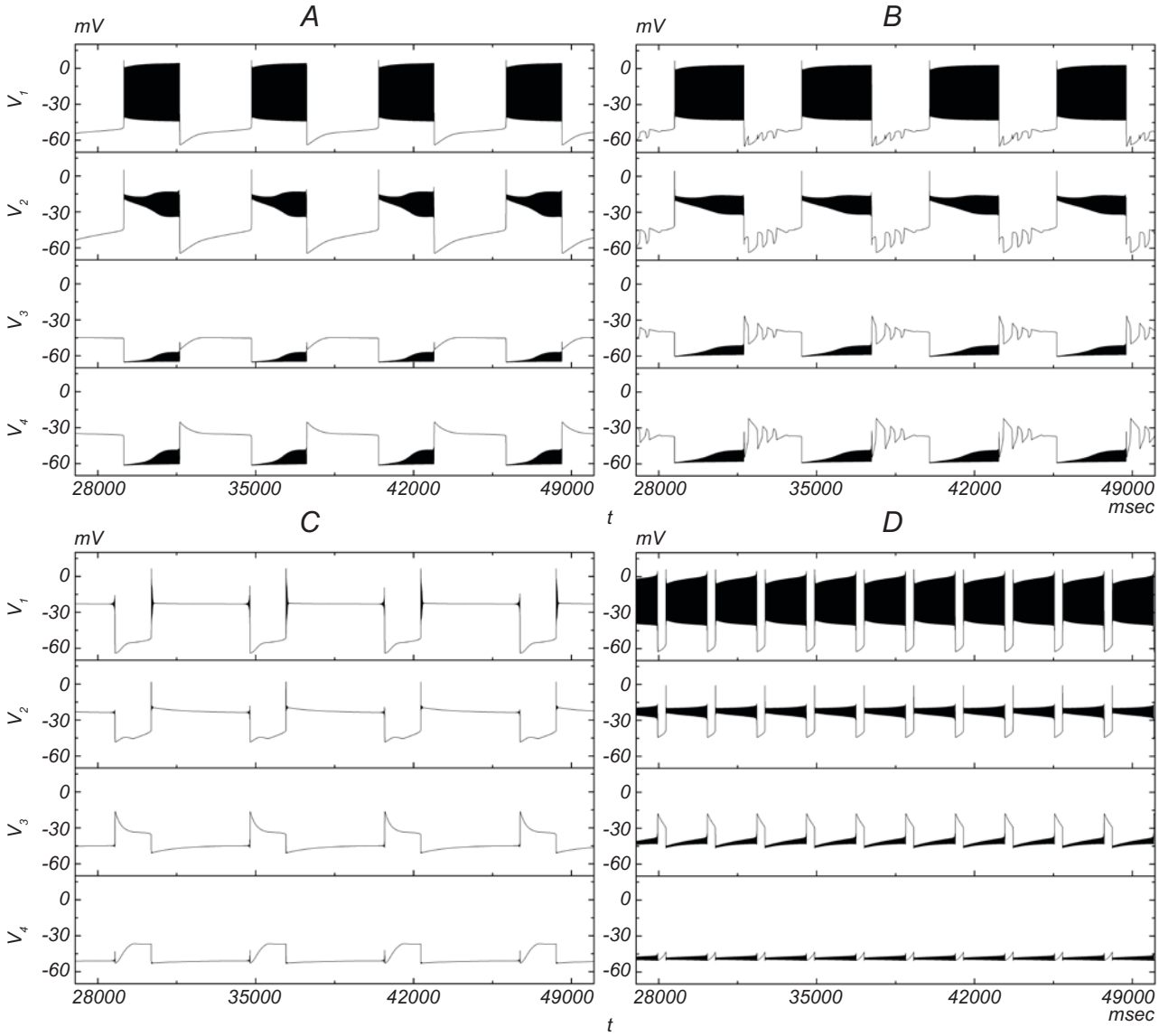

F i g. 4. The potassium conductance g_k in pre-I neuron is set to 8 nS. The tonic drive d1 value in A-D are 0.3, 0.6, 1.5, and 2, respectively.

the N_3 and N_4 neurons were strongly inhibited, and *vice versa*. In summary, variations in the d_1 to different neurons in the network influenced the firing pattern and the overall oscillatory period.

Influence of the Removal of Sodium Ion Channels or Synapses and Drives on Variation of the Firing Pattern in the Network. Physiological experiments demonstrated that some blockers, such as TTX or riluzole, can cause inactivation of certain ion channels [25, 26]. Application of the blockers in the physiological experiment in fact corresponds to the removal of the respective ion channels in numerical model presentation. It is essential for us to make clear the impact of certain channels on the network functioning.

Note that A in Fig. 5 is the original drawing under conditions of the default parameters. Primarily, the effect of the removal of sodium ion channels from pre-I neuron can be researched (B). It is obvious that the bursting pattern or subthreshold oscillations have already vanished, compared to A. Therefore, the sodium ion channels in pre-I neuron may be a pivotal element for generating bursting activity. Then, in panel C, sodium ion channels were removed from the early-I neuron. From this graphs, two conclusions can be made. One is that the firing

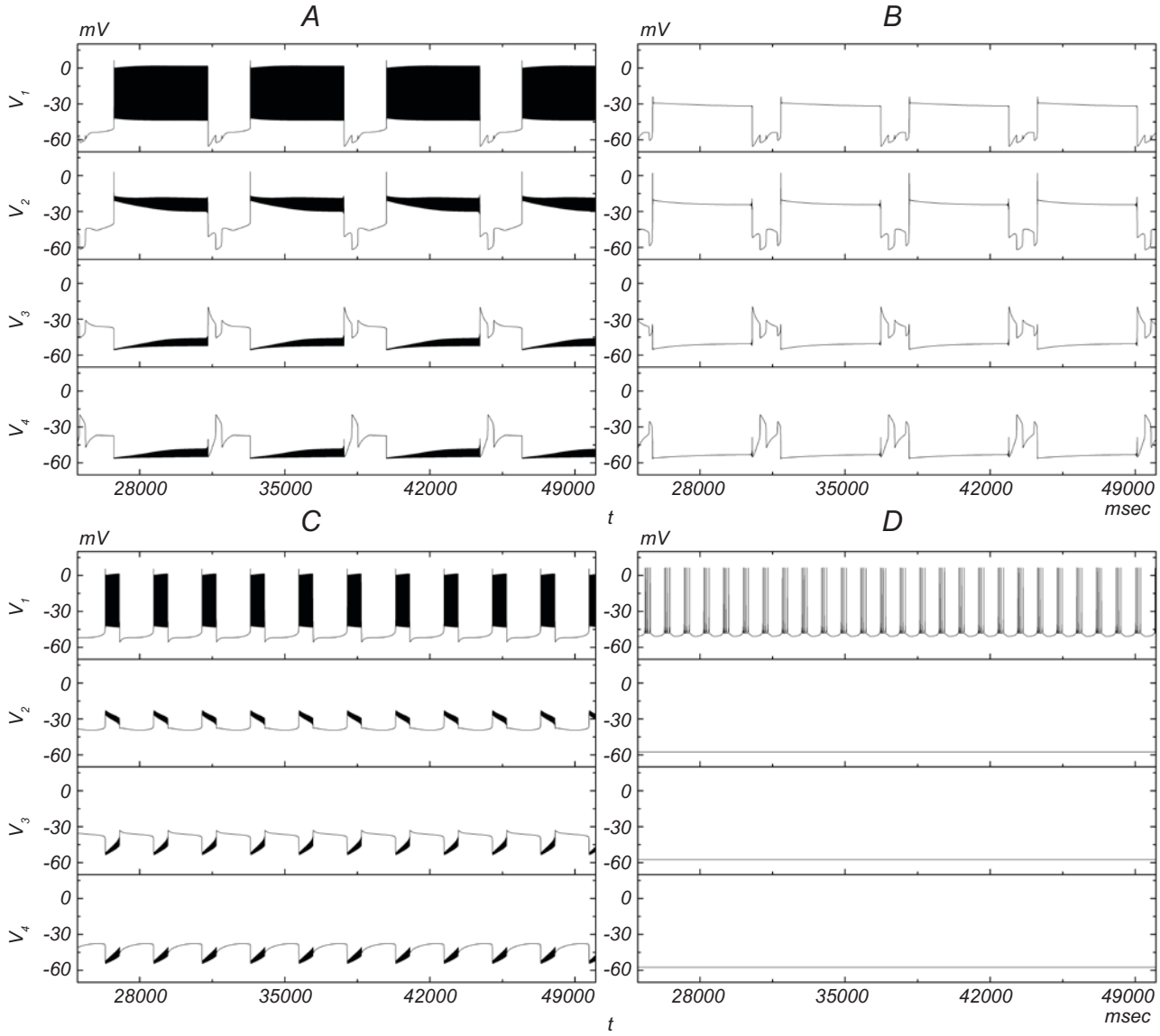

F i g. 5. Firing patterns of the network after the removal of certain ion channels. A) Original drawing. B) Removal of the sodium ion channels in the pre-I neuron. C) Removal of these channels in the early-I neuron. D) Removal of all tonic drives and synapses between the neurons to let them be independent of each other.

periods became shorter. Another one is that the parts that connect the bursting pattern or subthreshold oscillations change from an oscillation mode to smoothness. Finally, the phenomenon in seen in panel D is described. Each neuron is isolated, and the latter three neurons have tended to obtain the resting potential, except the pre-I neuron. As the pre-I neuron generates stable bursting activity, it can be concluded that this cell is actually a pacemaker unit that is responsible for the spontaneous firing pattern.

Biparametric Screening Plane with Two Bifurcation Parameters, g_{SynE1} and g_{NaP}. Here, we present plots of the (g_{SynE1}, g_{NaP}) parameter space displaying the dynamic behavior of the pre-I neuron in the network, which was obtained by calculating NSs. In Fig. 6, the panel is comprised of 101*101 points on a homogeneous grid within the given parameter range; namely, for this plot, no less than 104 simulations have been computed. The color-scale bar at the right in the inset of the figure yields NSs running from 1 (tonic spiking) to 11 (bursting), and the noninterger regions stand for aperiodic bursting. It is clearly observable that there are boundaries of the spike-adding cascade of the model. Figure 6 elaborates different kinds of the

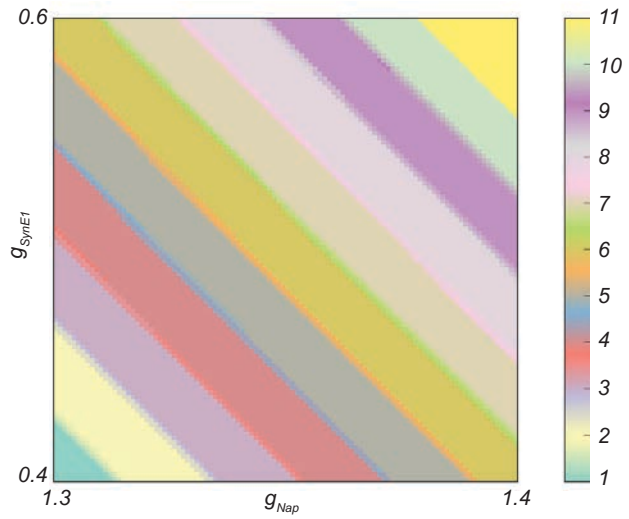

F i g. 6. The number of spikes per burst (NS) was plotted as the dependence on the g_{SynE1} and g_{NaP}. The respective biparametric screening plane (g_{SynE1}, g_{NaP}) clearly demonstrates that the phases of the spike-adding cascade and regions of aperiodic bursting are scattered and separated by boundaries (shown by distinct colors). The color bar at the right gives the spike number per burst scaling from 1 to 11. The number 1 denotes tonic-spiking, numbers 2-11 represent regular bursting, and noninteger regions correspond to aperiodic bursting.

firing patterns that could exist according to different pairs of the parameters. For a given g_{SynE1}, the increase in the g_{NaP} may lead to the NSs increasing by unity, while for a given g_{NaP}, the NS increases by the unity as the g_{SynE1} increases. An interesting phenomenon is that the plot does not contain chaotic regions but appears to show aperiodic bursting.

DISCUSSION

In this research, we have studied how different parameters or structure of the network affect the firing pattern in the computational model of the simplified respiratory network. From the results, we draw some conclusions presented below.

(i) In the case of pre-I neuron taken without the network, the characteristics that it shows can be observed in isolation. When we take the E_{Na} and E_K as examples, the change in their values depicts the possibility of highly abundant firing patterns, such as period-adding bifurcation, period-doubling bifurcation, and chaotic regions.

(ii) After subjecting pre-I neuron to AC stimulation and adjusting various stimulus strengths, i.e., the amplitude and frequency, we can find the following. The figures exhibit a lot of strange firing patterns, in particular irregular and periodic firing ones.

(iii) The tonic drive coming d_1 from the pons as one of the three main tonic drivers must incessantly influence the respiratory rhythm. When the potassium conductance value was set to 8 nS, depending upon the adjusting the d_1 value, variations of the membrane potential led to bursting-spiking or spiking-bursting transitions.

(iv) After removing the sodium channels from neurons N_1 and N_2, respectively, or breaking each neuronal connection in the network, it can be concluded that the lack of sodium channels in N_1 will cause the disappearance of the bursting pattern, while the lack of sodium channels in N_2 will cause shortening of the firing period. After breaking of neuron-to-neuron connections in the network, only the pre-I neuron can produce firing; others remain in the resting state.

(v) By depicting the biparametric screening plane with the g_{SynE1} and g_{NaP} and choosing suitable ranges for these two parameters, we obtain a figure with different color graduations. According to the color-scale bar at the right of the inset in the figure, the range of NSs runs from 1 (tonic spiking) to 11 (bursting), and the noninterger regions stand for aperiodic bursting.

Based on the findings mentioned above, we gain a more in-depth understanding of the role of the respiratory network in the modulation of the neuronal firing pattern. In this paper, several computationally effective tools including voltage waveforms, evaluations of ISIs, and approaches with respect to NSs, have been tested. We combined 1D and 2D parametric planes of the complicated dynamics of the respiratory network and were able to give detailed explanations for various spike-addition/deletion cascades and various transitions between firing patterns. To date, the number of studies on respiratory neurons and their kinds in the respiratory network remain limited, and an effort should be made in the future to broaden the applicability of the computing methods suggested here for the investigation of larger neuronal networks.

Acknowledgments. This work was supported by the National Natural Science Foundation of China under the Grant Nos. 11572127 and 11172103.

This study was carried out with the use of computer modeling; thus, confirmation of the correspondence to the existing ethical standards for the experiments on animals is not necessary.

The authors, Y. Zhang, Sh. Liu, and D. Xiong, declare the absence of any conflict in commercial or financial relations, relationships with organitations or persons that in any way could be related to the study, and also in interrelations of the co-authors.

REFERENCES

1. T. Lumsden, "Observations on the respiratory centres in the cat," *J. Physiol.*, **57**, 153-160 (1923).
2. F. E. Bloom and V. B. Mountcastle, *Intrinsic Regulatory Systems of the Brain*, Vol. 4, American Physiological Society (1986).
3. D. W. Richter, D. Ballantyne, and J. E. Remmers, "How is the respiratory rhythm generated? A model," *Physiology*, **1**, 109-112 (1986).
4. C. von Euler, "Brain stem mechanisms for generation and control of breathing pattern," in Suppl. 11, Handbook of Physiology, The Respiratory System, Control of Breathing, *Compehens. Physiol.* (1986).
5. A. L. Bianchi, M. Denavit-Saubie, and J. Champagnat, "Central control of breathing in mammals: neuronal circuitry, membrane properties, and neurotransmitters," *Physiol. Rev.*, **75**, 1-45 (1995).
6. I. A. Rybak, A. P. L. Abdala, and S. N. Markin, "Spatial organization and state-dependent mechanisms for respiratory rhythm and pattern generation," *Prog. Brain Res.*, **165**, 201-220 (2007).
7. J. C. Smith, A. P. L. Abdala, H. Koizumi, et al., "Spatial and functional architecture of the mammalian brain stem respiratory network: a hierarchy of three oscillatory mechanisms," *J. Neurophysiol.*, **98**, 3370-3387 (2007).
8. J. C. Smith, A. P. L. Abdala, I. A. Rybak, et al., "Structural and functional architecture of respiratory networks in the mammalian brainstem," *Philos. Trans. R. Soc. Lond. Ser. B, Biol. Sci.*, **364**, 2577-2587 (2009).
9. J. C. Smith, A. P. L. Abdala, A. Borgmann, et al., "Brainstem respiratory networks: building blocks and microcircuits," *Trends Neurosci.*, **36**, 152-162 (2013).
10. G. F. Alheid, W. K Milsom, and D. R. McCrimmon, "Pontine influences on breathing: an overview," *Respir. Physiol. Neurobiol.*, **143**, 105-114 (2004).
11. R. M. Harper, M. A. Woo, and J. R. Alger. "Visualization of sleep influences on cerebellar and brainstem cardiac and respiratory control mechanisms," *Brain Res. Bull.*, **53**, No. 1, 125-131 (2000).
12. A. von Leupoldt, A. Keil, P. Y. S. Chan, et al., "Cortical sources of the respiratory-related evoked potential," *Respir. Physiol. Neurobiol.*, **170**, No. 2, 198-201 (2010).
13. M. I. Cohen, "Neurogenesis of respiratory rhythm in the mammal," *Physiol. Rev.*, **59**, No. 4, 1105-1173 (1979).
14. W. Wang, M. L. Fung, and W. M. St John, "Pontile regulation of ventilatory activity in the adult rat," *J. Appl. Physiol.*, **74**, No. 6, 2801-2811 (1993).
15. J. S. Jodkowski, S. K. Coles, and T. E. Dick, "A 'pneumotaxic centre' in rats," *Neurosci. Lett.*, **172**, No. 1, 67-72 (1994).
16. S. F. Morrison, S. L. Cravo, and H. M. Wilfehrt, "Pontine lesions produce apneusis in the rat," *Brain Res.*, **652**, No. 1, 83-86 (1994).
17. W. M. S. John, "Neurogenesis of patterns of automatic ventilatory activity," *Prog. Neurobiol.*, **56**, No. 1, 97-117 (1998).
18. J. Duffin, "A commentary on eupnoea and gasping," *Respir. Physiol. Neurobiol.*, **139**, No. 1, 105-111 (2003).
19. W. M. S. John and J. F. R. Paton, "Defining eupnea," *Respir. Physiol. Neurobiol.*, **139**, No. 1, 97-103 (2003).
20. J. C. Smith, R. J. Butera, N. Koshiya, et al., "Respiratory rhythm generation in neonatal and adult mammals: the hybrid pacemaker–network model," *Respir. Physiol.*, **122**, No. 2, 131-147 (2000).
21. Y. I. Molkov, N. A. Shevtsova, C. Park, et al., "A closed-loop model of the respiratory system: Focus on hypercapnia and active expiration," *PloS One*, **9**, No. 10, e109894 (2014).
22. J. E. Rubin, B. J. Bacak, Y. I. Molkov, et al., "Interacting oscillations in neural control of breathing: modeling and qualitative analysis," *J. Comput. Neurosci.*, **30**, No. 3, 607-632 (2011).
23. I. A. Rybak, J. F. R. Paton, and J. S. Schwaber, "Modeling neural mechanisms for genesis of respiratory rhythm and pattern. I. Models of respiratory neurons," *J. Neurophysiol.*, **77**, No. 4, 1994-2006 (1997).
24. J. E. Rubin, N. A. Shevtsova, G. B. Ermentrout, et al., "Multiple rhythmic states in a model of the respiratory central pattern generator," *J. Neurophysiol.*, **101**, No. 4, 2146-2165 (2009).
25. J. F. Paton, A. P. Abdala, H. Koizumi, et al., "Respiratory rhythm generation during gasping depends on persistent sodium current," *Nat. Neurosci.*, **9**, No. 3, 311-314 (2006).
26. I. A. Rybak, K. Ptak, N. A. Shevtsova, et al., "Sodium currents in neurons from the rostroventrolateral medulla of the rat," *J. Neurophysiol.*, **90**, No. 3, 1635-1642 (2003)
27. R. J. Butera, J. Rinzel, and J. C. Smith, "Models of respiratory rhythm generation in the pre-Bötzinger complex. I. Bursting pacemaker neurons," *J. Neurophysiol.*, **82**, No. 1, 382-397 (1999).
28. M. M. Ali, K. K. Sellers, and F. Fröhlich, "Transcranial alternating current stimulation modulates large-scale cortical network activity by network resonance," *J. Neurosci.*, **33**, No. 27, 11262-11275 (2013).

29. R. F. Helfrich, T. R. Schneider, S. Rach, et al., "Entrainment of brain oscillations by transcranial alternating current stimulation," *Curr. Biol.*, **24**, No. 3, 333-339 (2014).
30. T. Neuling, S. Rach, and C. S. Herrmann., "Orchestrating neuronal networks: sustained after-effects of transcranial alternating current stimulation depend upon brain states," *Front. Human Neurosci.*, **7**, No. 1, 161 (2013).
31. K. L. Kilgore and N. Bhadra, "Nerve conduction block utilizing high-frequency alternating current," *Med. Biol. Eng. Comput.*, **42**, No. 3, 394-406 (2004).